McMullen, M. D., Shaw, P. A., & Martin, T. E. (1979) *J. Mol. Biol. 132*, 679–694.
Muthukrishnan, S., Morgan, M., & Banerjee, A. K. (1976) *Biochemistry 15*, 5761–5768.
Ordahl, C. P., & Caplan, A. I. (1978) *J. Biol. Chem. 253*, 7683–7691.
Ouellette, A. J., & Malt, R. A. (1979) *Am. J. Physiol. 237*, R360–R365.
Ouellette, A. J., & Ordahl, C. P. (1981) *J. Biol. Chem. 256*, 5104–5108.
Ouellette, A. J., Kumar, A., & Malt, R. A. (1976) *Biochim. Biophys. Acta 425*, 384–395.
Ouellette, A. J., Ordahl, C. P., & Van Ness, J. (1980) *J. Cell Biol. 87*, 277a.
Ouellette, A. J., Silverberg, M. B., & Malt, R. A. (1981) *Biochemistry 20*, 3561–3567.
Pelham, H. R. B., & Jackson, R. J. (1976) *Eur. J. Biochem. 67*, 247–256.
Perry, R. P., & Kelley, D. E. (1968) *J. Mol. Biol. 35*, 37–59.
Perry, R. P., Latorre, J., & Kelley, D. E. (1972) *Biochim. Biophys. Acta 262*, 220–226.
Ross, J. A., Malamud, D., Caulfield, J. B., & Malt, R. A. (1975) *Am. J. Physiol. 229*, 952–954.
Rudensey, L. M., & Infante, A. I. (1979) *Biochemistry 18*, 3056–3063.
Rudland, P. S., Weil, S., & Hunter, A. R. (1975) *J. Mol. Biol. 96*, 745–766.
Schochetman, G., & Perry, R. P. (1972) *J. Mol. Biol. 63*, 577–590.
Sonenshein, G. E., & Brawerman, G. (1977) *Eur. J. Biochem. 73*, 307–312.
Spirin, A. S. (1969) *Eur. J. Biochem. 10*, 20–35.
Spirin, A. S., Belitsina, N. V., & Lerman, M. I. (1965) *J. Mol. Biol. 14*, 611–615.
Spohr, G., Granboulan, N., & Morel, C. (1970) *Eur. J. Biochem. 17*, 296–318.
Strohman, R. C., Moss, P. S., & Micou-Eastwood, J. (1977) *Cell (Cambridge, Mass.) 10*, 265–273.
Van Ness, J., Maxwell, I. H., & Hahn, W. E. (1979) *Cell (Cambridge, Mass.) 18*, 1341–1349.
Wilt, F. H. (1973) *Proc. Natl. Acad. Sci. U.S.A. 70*, 2345–2349.

Optical Model Studies of Salt-Induced Conformational Transitions in the Nucleosome†

Rodney E. Harrington

ABSTRACT: Optical modeling of the DNA conformation has been used to interpret the results of highly sensitive flow birefringence and extinction angle studies on nucleosome core particles over a range of counterion strength (using KCl as the supporting electrolyte) from <0.15 mM to >0.6 M. Results are consistent with an oblate disk or wedge of axial ratio $p^{-1} \simeq 2$ over an intermediate salt concentration range from about 1.5 to 450 mM. Below ~1.5 mM, the particle appears to unfold into an extended prolate or oblate structure which can be modeled as a uniform superhelix of DNA. Above ~0.45 M, the particle unfolds into a conformation which is hydrodynamically similar to but optically quite different from the low-salt structure. This form can be modeled as a partially unfolded disk in which only the nucleosomal DNA ends become dissociated and the central region remains bound to the histone core. A description of the optical modeling methods is presented, and the results are correlated with hydrodynamic property changes.

A fascinating question related to the molecular architecture of eukaryotic chromatin is the seemingly paradoxical fact that transcription can occur readily even though the DNA is packaged with extraordinary efficiency. A typical nucleus may contain 2 m of DNA with a packing ratio of 10^4 to 1. In *Escherichia coli*, RNA polymerase may bind to promoter regions as large as 30–40 base pairs [for a review, cf. Siebenlist et al. (1980)], and insofar as these concepts apply also to eukaryotic systems [cf. Ziff (1980)], it is clear that significant structural changes must occur in active chromatin [for a review, cf. Mathis et al. (1980)]. At the nucleosomal level, altered conformational states have been reported in replicating (Seale, 1978) and in transcriptionally active (Weintraub & Grondine, 1976; Garel & Axel, 1976) chromatin. Furthermore, the role of RNA polymerase activity seems to be modulated by salt concentration (Williamson & Felsenfeld, 1978; Wasylik & Chambon, 1979; Wasylik et al., 1979). Hence, the question of salt-dependent nucleosomal structures seems to be relevant to an understanding of transcriptional processes at the molecular level.

Conformational transitions in nucleosomes have been observed in solution under extremes in ionic strength conditions. Single transitions at ionic strengths of around 1 mM or less have been reported by Libertini & Small (1980), Dieterich et al. (1979, 1980), and Wu et al. (1979) and around 5 mM by Dieterich et al. (1980) and Martinson et al. (1979). Two defined transitions have been reported by Gordon et al. (1978, 1979) and in an earlier communication from this laboratory (Harrington, 1981). These transitions occur also around 1 and 5–7 mM salt. A conformationally metastable region appears to exist from about 10 to 350 mM ionic strength, and an additional broad transition is observed between approximately 0.4 and 0.6 M salt (Dieterich et al., 1979; Wilhelm & Wilhelm, 1980; McGhee et al., 1980). Below ~0.6 M, the nucleosome evidently remains intact, but at higher salt concen-

† From the Department of Chemistry, University of Nevada, Reno, Reno, Nevada 89557. *Received June 10, 1981.* This research was sponsored by National Science Foundation Research Grant PCM 7905609.

0006-2960/82/0421-1177$01.25/0

trations, significant dissociation of histone core components is found to occur (Stacks & Schumaker, 1979).

Both the high- and low-salt forms of the nucleosome are of interest since these may mimic in vivo conformational changes in active chromatin. These transitions appear to be mediated entirely by the supporting counterion concentration, and hence, they must occur as a result of changes in electrostatic interactions within the core itself due to counterion screening effects. It is therefore reasonable to suppose that at very low ionic strengths electrostatic effects involving phosphate charges on the DNA and charged residues in the histone polar regions are maximal. At very high ionic strengths, these charges will be highly screened and the corresponding electrostatic interactions greatly reduced.

The core histones are known to undergo chemical modifications including methylation, acetylation, phosphorylation, covalent binding to ubiquitin, and ADP ribosylation (Isenberg, 1979). Acetylation of lysine residues reduces the positive charge of the amino-terminal region, while phosphorylation entails the attachment of a phosphate ester to a serine residue in the amino-terminal region. Both effects may be qualitatively mimicked by high-salt conditions in solution. All four core histones are acetylated and phosphorylated at some point during the cell cycle (Dixon et al., 1975), and tetraacetylation of histone H4 has been correlated in detail with transcriptional activity (Chahal et al., 1980). This level of modification reduces the overall positive charge on H4 from ~20 to ~16 and that in the amino-terminal region from ~10 to ~6 (McGhee & Felsenfeld, 1980). Hence, electrostatic changes at the nucleosomal level do occur in active chromatin, although the effects are complicated and are still not well understood.

In a prior communication from this laboratory, I have used streaming birefringence along with classical optical modeling methods to assess possible conformational states of the nucleosome at low salt concentration (Harrington, 1981). Transitions similar to those reported by Gordon et al. (1978, 1979) were observed. The preparations used in all studies in which multiple low-salt transitions have been observed contained some polydispersity, however, and it has been shown that DNA lengths greater than ~170 nucleotide pairs (np)[1] can be associated with a fairly broad conformational transition centered around 7 mM salt (Dieterich et al., 1980).

In the present work, I have used the streaming birefringence methodology to characterize highly monodisperse 146-np DNA core particles over a counterion strength range from <0.15 mM to 0.6 M. KCl is used as a supporting electrolyte. A single low-salt transition is observed between ~0.15 and 1 mM, centered at approximately 0.5 mM KCl. This transition appears virtually identical with the lower salt transition reported previously (Harrington, 1981). A second transition is observed between ~0.4 and 0.6 M KCl which seems conformationally different from the one at low salt concentration. Models for these states which are consistent with the opticohydrodynamic data are proposed. Preliminary experimental results on the high-salt transition have been reported previously (Harrington, 1980).

Materials and Methods

Preparation of Core Particles. Mononucleosome cores were prepared from fresh, mature chicken erythrocytes by using appropriate modifications to the Hewish & Burgoyne (1973) and Lutter (1978) methods as developed by Bunick (G. Bunick, unpublished experiments). These procedures led to stable preparations of core particles containing 146 ± 4-np DNA (G. Bunick, unpublished experiments) and a normal complement of core histones (Figure 1). Major modifications to the Lutter (1978) procedure were as follows. (a) Erythrocytes were obtained from fresh chicken blood by centrifugation and were lysed by washing 4 times in buffer A (0.34 M sucrose containing 2 mM EDTA, 0.5 mM EGTA, 0.1 mM PMSF, 0.2% 2-propanol, and 0.5% NP-40, pH 7.4). (b) The nuclei were digested with 45 units/mL micrococcal nuclease (Worthington). (c) Stripping the soluble chromatin was done with 0.194 volume of 4 M NaCl added dropwise with stirring at 0 °C followed by addition of 3% sucrose. The stripping column was preequilibrated with 0.65 M NaCl, 5 mM Tris, 0.2 mM BME, and 0.02% sodium azide, pH 7.5. (d) After digestion of soluble chromatin, the sample was made 3.2% sucrose–0.02% sodium azide, and the monomer fraction was obtained by gel filtration on Sephacryl S-300 (Pharmacia Fine Chemicals). (e) Pooled monomer fractions were dialyzed against a Mg precipitation buffer (100 mM KCl, 12 mM $MgCl_2$, 1 mM Pipes, 3 mM sodium azide, 0.1 mM PMSF, and 0.2% 2-propanol). The dialysate was centrifuged at ~8000*g* for 20 min and the supernatant dialyzed against a storage buffer (5 mM Tes, 20 mM NaCl, 0.2 mM EDTA, 3 mM sodium azide, 0.1 mM PMSF, and 0.2% 2-propanol). The core particles were concentrated to 100–200 A_{260} units in a collodion bag apparatus (M_r cutoff 24 000) and stored at refrigerator temperature. Although the particles appeared to be stable for several months under these conditions as characterized by hydrodynamic properties and CD, the results reported here were obtained on particles stored no longer than 3 weeks. No core particles used in the present work were frozen except as noted specifically.

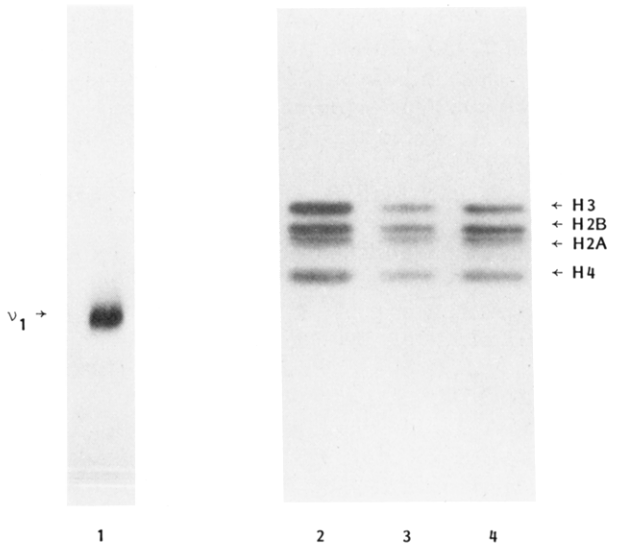

FIGURE 1: Gel electrophoresis of core particles at various counterion strengths. Lane 1, particle gel of intact core particle sample used in the present work; lanes 2, 3, and 4, $NaDodSO_4$ gel electrophoresis of inner histones for core particles at 6, 100, and 600 mM counterion strength, respectively.

Gel Electrophoresis. All gels were run in a Hoefer SE 620 slab gel apparatus (Hoefer Scientific Instruments) with gels 1.5 mm × 14 cm and either 16 or 32 cm long. Destaining was by diffusion. (a) Particle gels were 16 cm long and consisted of 6% acrylamide–3.5% bis(acrylamide) in 1/5 × TBE buffer (0.45 M Tris, 0.45 M boric acid, and 12.5 mM EDTA, pH 8.3). Gels were loaded with 30–40 μg/lane, were run at 200

[1] Abbreviations: EDTA, ethylenediaminetetraacetic acid; EGTA, ethylene glycol bis(β-aminoethyl ether)-*N,N,N',N'*-tetraacetic acid; BME, β-mercaptoethanol; PMSF, phenylmethanesulfonyl fluoride; Pipes, 1,4-piperazinediethanesulfonic acid; Tes, 2-[[tris(hydroxymethyl)-methyl]amino]ethanesulfonic acid; $NaDodSO_4$, sodium dodecyl sulfate; CD, circular dichroism; np, nucleotide pair.

V for 2–2.5 h with regulation to 25 °C, and were stained with Coomassie Blue R-250. (b) Histones were run on $NaDodSO_4$ disc gels as described by Laemmli (1970). Gels were 16 cm long, 5% bis(acrylamide)–acrylamide stacking and 15% bis(acrylamide) running, respectively. Particles were started at 100 V for 20 min, were run at 200 V for 50 min regulated to 4 °C, and were stained with Coomassie Blue R-250. (c) Denatured DNA gels were used to monitor chromatin digestion and to locate monomer fractions as described. Samples were denatured by boiling in 10 M urea, 2% $NaDodSO_4$, and 1/50 TBE buffer, and 20–35 μL was loaded on 16 cm long 8% acrylamide–3% bis(acrylamide) gels 7 M in urea and 0.1% $NaDodSO_4$. These were run 90 min at 300 V with regulation to 20 °C. Staining was 2 h in 0.01% toluidine blue in 40% methanol.

Pyrene Excimer Fluorescence Studies. Pyrene excimer fluorescence at 460 nm was monitored as a function of KCl concentration by labeling the H3 cysteine-110 residues with *N*-(3-pyrenyl)maleimide as described earlier (Zama et al., 1977). After attachment of the sulfhydryl probe at 1.4 M KCl, the core particles were step dialyzed down to the final salt concentration in 0.1–0.2 M increments of several hours duration, followed by ultracentrifugal fractionation in a 5–25% sucrose gradient and final equilibrium dialysis against pure solvent. Fluorescence intensities were determined by using a Perkin-Elmer MPF 44A fluorescence spectrometer with excitation at 340 nm.

Streaming Birefringence and Intrinsic Viscosity. Flow birefringence measurements were made at shear rates between 1 and 16 ks^{-1} with a special highly sensitive photoelectric scanning instrument developed in this laboratory. Details have been given elsewhere on the instrument (Harrington, 1970a,b, 1979) and on its use in the present application (Harrington, 1979, 1981). Computerized data reduction and signal averaging methods were employed as described elsewhere (Barrett & Harrington, 1977) because of the intense optical noise and very small particle orientation observed over the nonturbulent shear range of the flow cell.

Intrinsic viscosities were determined with a cartesian diver, Couette-type viscometer (Gill & Thompson, 1967; Harrington, 1970a,b). All experimental data are at 25 °C.

KCl was used in all studies as a supporting electrolyte. Stock solutions of core particles were equilibrium dialyzed into 1 mM Tris-HCl and either 0.03 or 0.2 mM EDTA. The lower EDTA concentration was used to prepare samples at ionic strengths <5 mM. All samples were made by direct dilution into pure KCl solutions. Glass-distilled water was used for all solutions and to rinse the flow cell and other apparatus between runs. Five replicate runs on each sample were made with overnight dialysis against pure solvent between runs. Other experimental parameters were as given previously (Harrington, 1981).

Theory

Flow Birefringence and Treatment of Data. A critique and full description of the method and the underlying theory have been given elsewhere (Harrington, 1967, 1970b, 1979, 1981; Oriel & Schellman, 1966). For purposes of the present discussion, I include a brief recapitulation here.

The principal experimental quantities are the extinction angle, the flow birefringence, and the intrinsic viscosity. The extinction angle is the mean orientation angle of an oriented particle in a shear field and is exclusively a hydrodynamic property. Peterlin & Stuart (1939) have given a hydrodynamically rigorous (Oriel & Schellman, 1966) treatment of the extinction angle for rigid ellipsoids of revolution. At moderate velocity gradients, this can be expressed as a quadratic polynomial in the ratio of shear rate to rotational diffusion coefficient, G/D_r. Peterlin and Stuart also have given orientation and optical theories for the flow birefringence of rigid ellipsoids by assuming coincidence of the principal optical and geometrical axes and the applicability of continuum dielectric theory to the birefringence. Combining these results with other aspects of rigid particle theory, one finds that (Harrington, 1970b, 1979, 1981)

$$\frac{[n]}{[\eta]} = \frac{4\pi\bar{v}Md}{5n\delta RT}(g_a - g_b) \tag{1}$$

in which $[n] = [\Delta n/(cG\eta_0)]_{c,G\to 0}$ is the Maxwell coefficient, Δn is the experimental flow birefringence, c is the weight concentration, η_0 is the absolute solvent viscosity, $[\eta]$ is the intrinsic viscosity, $\bar{v}$ is the partial specific volume of the particle, M is its molecular weight, d and δ are functions of its axial ratio p and oblate or prolate symmetry only, n is the refractive index of the solution, and the g_i values are excess polarizability components per unit volume for the birefringent solution. For rigid ellipsoids, eq 1 predicts that the optical factor $g_a - g_b$ is directly determined as a function of axial ratio in terms of experimental parameters only.

The g_i values are also related to the refractive index increment of the solution for solute particles of ellipsoidal or cylindrical symmetry (Harrington, 1970b):

$$\frac{dn}{dc} = \frac{2\pi\bar{v}}{3n}(g_a + 2g_b) \tag{2}$$

Hence, an independent measurement of dn/dc enables g_a and g_b to be evaluated separately. These can be related to the corresponding refractive index components n_a and n_b of the particle by using macroscopic continuum dielectric theory

$$g_i = \frac{1}{4\pi}\frac{n_i^2 - n_0^2}{1 + [(n_i^2 - n_0^2)/n_0^2]L_i} \tag{3}$$

where n_0 is the solvent refractive index and the L_i values are ellipsoidal field shape factors (Harrington, 1981). In this way, the intrinsic birefringence of the solute particles themselves, $\Delta n_{int} = n_a - n_b$, can be isolated from the total observed flow birefringence. However, because of the dependence of d and δ in eq 1 upon particle symmetry and the axial ratio, Δn_{int} can only be determined as a function of these quantities.

The use of optical models to estimate the intrinsic birefringence of biological structures has been described as an augmentation and interpretive aid to the polarizing microscope (Inoue, 1961) and to characterize the packing of DNA in virus particles (Maestre & Kilkson, 1965) and in nucleosomes (Harrington, 1979, 1981). Standard dielectric theory gives the real refractive index component along a principal optical axis in terms of the polarizability per volume (γ_i):

$$n_i^2 = 1 + 4\pi\gamma_i \tag{4}$$

Hence, the intrinsic birefringence of the models can be estimated by assuming tensoral additivities of γ_i in proposed model structures.

In the present work, it is assumed that the DNA conformation and trajectory in the nucleosome are the principal determinants of the optical anisotropy. This assumption seems justified because of the very large intrinsic anisotropy of DNA relative to that of most globular proteins (Harrington, 1981). In addition, the experimental anisotropy of DNA from flow birefringence (Harrington, 1970b) is used in calculating the intrinsic birefringence of optical nucleosome models by using

Table I: Ionic Strength Dependence of Various Experimental Parameters Used in This Work

ionic strength	ρ_0 (g/cm^3)	$\eta_0 \times 10^2$ (P)	n_0	$s^0_{20,w}$ (S)[a]	$[\eta]$ (cm^3/g)	$\beta \times 10^{-6}$ [b]
0.006	0.99737	0.8928	1.33305	11.3	11.50	2.41
0.40	1.01581	0.9219	1.33696	9.8	13.96	2.39
0.50	1.02043	0.9300	1.33794	9.6	19.00	2.64
0.60	1.02502	0.9383	1.33891	9.4	36.00	3.25

[a] Wilhelm & Wilhelm (1980). [b] Calculated with $\bar{\nu} = 0.661$ at all salt concentrations (see text).

eq 4. In this way, any serious deficiencies in the optical theory, i.e., the inability of eq 1–3 to partition correctly the total birefringence into its intrinsic and form components, will be minimized or eliminated.

Results and Discussion

Representative experimental values of $[\eta]$, n_0, ρ_0, and η_0 as functions of total ionic strength are given in Table I. Experimental values of dn/dc were not found to change significantly over the salt concentration range studied, and the value $dn/dc = 0.184$ was used in all calculations. The ratio $[n]/[\eta]$ is plotted against ionic strength in Figure 2. Two distinct transitions are observed: one which occurs below ~1 mM and one above ~0.4 M. The two transitions are not easily distinguished in terms of intrinsic viscosity only since this property is very nearly the same at both extremes of the ionic strength range, but the intrinsic viscosity is significantly reduced at intermediate salt concentrations. This implies that both transitions occur with increasing anisometry with respect to rotational diffusion. Similar behavior is observed in the extinction angles.

Metastable Conformer at Intermediate Salt Concentrations Is Consistent with an Oblate Disk Model. The present results on core particles are qualitatively similar to previous studies on an earlier, more polydisperse nucleosome preparation (Harrington, 1981). In the earlier work, nucleosomes containing small amounts of DNA up to ~160 np were present. The additional 5–8 np on either end of the DNA may have been responsible for the slightly higher intrinsic viscosity at 0.1 M: $[\eta] = 12.8$ cm^3/g in that work and $[\eta] = 12.0$ cm^3/g here (Table I). Extinction angles were the same within the relatively large experimental scatter in both studies. The Maxwell coefficient at 0.1 M in the present work is also somewhat lower than that determined previously, however, so that the ratio $[n]/[\eta]$ is very nearly the same for both samples.

I have shown elsewhere (Harrington, 1979, 1981) that the observed $[n]/[\eta]$ ratio for the nucleosome at 0.1 M ionic strength is consistent with an optical model of 1.75 superhelical turns of DNA wound around an optically isotropic histone core with a superhelical pitch of 31 Å. This corresponds to an oblate particle with $p^{-1} \simeq 2$. The present results on core particles are entirely consistent with this model, which is essentially that of Finch et al. (1977). This model has recently been corroborated by the neutron scattering results of Braddock et al. (1981). The present results are also in substantial accord with the transient electric dichroism studies of Crothers et al. (1978) under similar ionic strength conditions.

Single Transition Is Observed at Low Salt Concentrations. The low-salt transition is shown in Figure 2A. The birefringence of the initial and final conformers is similar to that reported earlier with polydisperse samples (Harrington, 1981), but the transition itself is quite different. In the earlier work, I reported a substantial negative increase in $[n]/[\eta]$ over the salt range ~1 to ~10 mM, suggesting an optically distinct

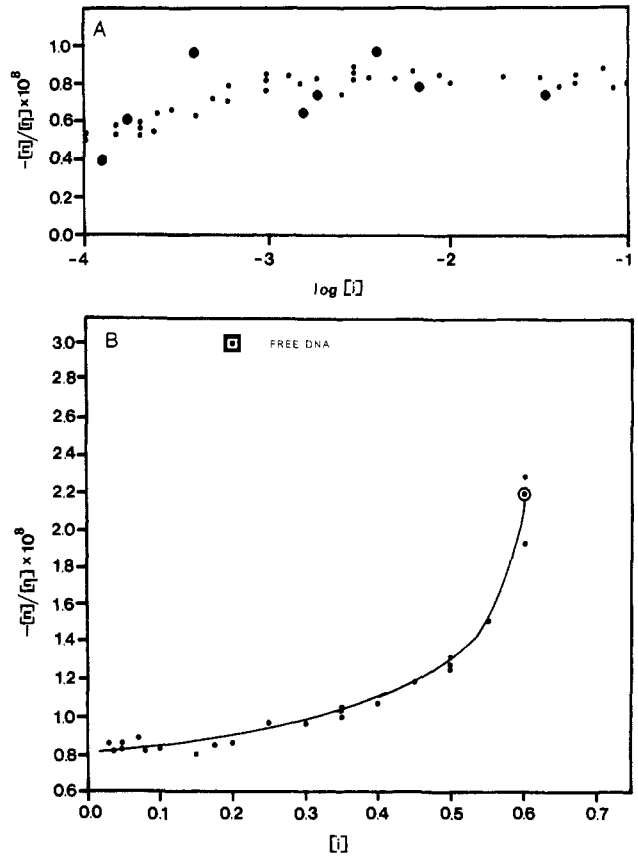

FIGURE 2: Dependence of the ratio of the Maxwell coefficient to the intrinsic viscosity, $[n]/[\eta]$, upon total counterion strength [i]. (A) $[n]/[\eta]$ vs. log [i] below ~100 mM. Large points represent core particles rapidly frozen to −78 °C and thawed rapidly in a 25 °C bath prior to study (see text). (B) $[n]/[\eta]$ vs. [i] at high salt concentration (>100 mM). The DNA point refers to free ~150-np DNA at 200 mM NaCl (Harrington, 1970b).

conformational state in this region with relatively abrupt transitions. Similar transitions and conformational states were observed also by Gordon et al. (1978, 1979). However, Figure 2A shows only a single broad transition which occurs over the range ~0.15 to >1 mM. The midpoint of this transition is somewhat lower than the low-salt transition previously observed, and the data in Figure 2A provide no evidence for an intermediate conformational state. Of the several reported low-salt transitions, Figure 2A corresponds most closely to the results of Libertini & Small (1980).

Possible reasons for the discrepancies in the number of low-salt transitional states have been presented and described in some detail (Harrington, 1981). It seems very likely that residual linker DNA is required to observe a second low-salt transition, a conclusion reached also by several other investigators (Dieterich et al., 1980; D. M. Crothers, unpublished experiments), since the only substantive differences between the previous study and the present one are in the nucleosome preparations themselves. However, at the present time, detailed mechanistic reasons for this must be regarded as speculative. The earlier nucleosome samples were prepared by using the Olins procedures (Olins, A. L., et al., 1977) in which nuclease digestion was of H1 unstripped chromatin and fractionation was by zonal ultracentrifugation followed by KCl precipitation and freezing to −20 °C. These samples showed some polydispersity in residual linker DNA sizes but contained a normal complement of core histones. Optical modeling of the birefringence between ~1 and ~10 mM salt in the earlier work suggested the possibility of a metastabilization of a partially unfolded transition state in this region, due possibly

to electrostatic effects associated with the residual linker DNA or to proteins bound to these regions. Such a conjecture is certainly not ruled out by the present results since the initial and final conformational states appear similar in both studies. An alternative possibility is that the intermediate form in the earlier study might have occurred as a consequence of freeze damage, possibly deriving from a conformational dislocation and destabilization of the histone core octamer. This possibility seems unlikely in view of the data on frozen nucleosomes included in Figure 2A. These results, indicated by heavy circles, were obtained by using core particles which had been frozen rapidly to −78 °C followed by thermal reequilibration to 25 °C. Although there is more scatter in these points than in the corresponding results on unfrozen particles, the two sets are in substantial agreement, and the heavy points certainly provide no indication of an intermediate conformational state above ~1 mM.

Low-Salt Conformer Is Consistent with an Extended Superhelical DNA Model. The value of $[\eta]/[\eta] \simeq -6 \times 10^{-9}$ (cgs units) below 0.15 mM is entirely consistent with my earlier result (Harrington, 1981) at the same ionic strength. Extinction angles for these samples are also similar to the earlier work and hence are not shown. Intrinsic viscosity data are given in Table I and are seen to be comparable although slightly lower in numerical value.

The birefringence corresponding to the lowest salt conformer in Figure 2A has been analyzed in terms of optical models (Harrington, 1981). Although the extinction angles are slightly greater with core particles in the present work, the results of the earlier optical analysis should nevertheless still be applicable. In the earlier study, the birefringence was shown to be consistent with extended prolate DNA superhelixes. Two equivalent models were proposed: one with $p = 7.3$ containing exactly 1.75 superhelical turns of DNA (plus residual DNA "tails" at either end) and a second with $p = 10.1$ containing exactly 152 np of DNA in the superhelix. The experimental birefringence was also consistent with an oblate model of $p^{-1} = 2.5$ similar to that proposed by Wu et al. (1979), although in this case, the extinction angle data were in far less satisfactory agreement.

The more extended superhelical model is attractive because it allows conservation of DNA–histone binding sites. If these are simple electrostatic interactions between the DNA and the polar histone regions, one might expect them to be relatively strengthened at low counterion strength. On the other hand, this picture also implies an intranucleosomal dissociation of the histone octamer. The association of histone oligomers under high salt conditions in solution is favored by increasing counterion concentration (Eikbush & Moudrianakis, 1978). In addition, Bradbury and co-workers (Bradbury et al., 1977) have demonstrated by using NMR and other physical methods that histone–histone interactions occur chiefly through the apolar regions with the basic amino-terminal regions relatively unaffected. If hydrophobic and other attractive interhistone interactions are moderated by electrostatic repulsion, the effect of low ionic strength may be simultaneously to stabilize DNA–histone attractions and to destabilize the histone core. This would be consistent with the conformational model proposed since the histone–DNA binding sites could be preserved, either specifically or nonspecifically, but the octameric integrity of the histone core (and hence the disk shape of the particle) would be lost. Such a picture would also be consistent with a separation of the sulfhydryls (cysteine-110 residue) in the H3 histones implied by the falloff in pyrene excimer fluorescence observed in Figure 4 below ~1 mM, and with

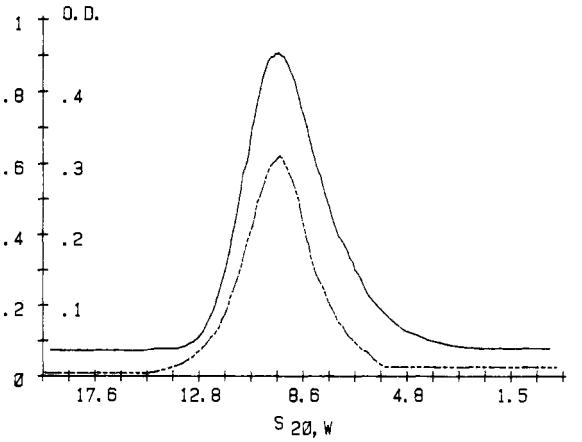

FIGURE 3: Sedimentation of core particles in 0.6 M KCl through a 5–25% sucrose gradient. Samples were the same core particle preparation used for the high-salt optical model analysis. Ordinate, OD at 260 nm (left-hand figures) and at 280 nm (right-hand figures). Abscissa, calculated $s_{20,w}$ for run conditions employed (28 000 rpm and 21 h in a Beckman SW-50 rotor). Peak scanning was with a LKB 2138 Uvicord S with a 0.1-mL cell. Solid curve, sample scanned at 260 nm. Dashed curve, replicate sample scanned at 280 nm.

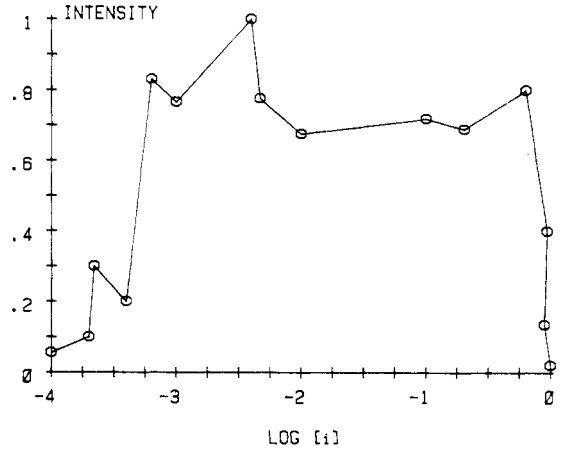

FIGURE 4: Fluorescence intensity relative to the highest reading (I) for the pyrene excimer fluorescence at 460 nm in core particles vs. log total counterion strength. Particles were labeled at the H3 sulfhydryls with *N*-(3-pyrenyl)maleimide as described earlier (Zama et al., 1977). Excitation wavelength, 340 nm. Lines shown connecting data points are arbitrary and are included only to help clarify general trends in the data. They do not necessarily possess interpolative significance.

a reasonable variant of the low-salt model proposed by Dieterich et al. (1979).

High-Salt Nucleosome Can Be Modeled as a Partially Unfolded Disk with an Intact Core. Figure 2B gives $[\eta]/[\eta]$ as a function of total counterion strength at high salt concentrations. Above ~0.2 mM salt, the data show a small increase, but above ~0.45 M, the large upward curvature seems clearly to imply a conformational transition in the nucleosome. Above ~0.6–0.65 M salt, the data become irreproducible, possibly due to histone loss (Dieterich et al., 1979; McGhee et al., 1980), with values approaching that of pure ~150-np DNA (Harrington, 1970b). Indeed, histone gel electrophoresis shows considerable core histone loss in samples whose $[\eta]/[\eta]$ ratios lie numerically above those in Figure 2B. However, all data reported here were obtained on samples having normal histone and particle gel patterns (Figure 1) and which showed single peaks when sedimented through a 5–25% sucrose gradient (Figure 3). From Figure 3, a slowly sedimenting component of $S \simeq 4$–5 could be detected at a concentration of ~10% or less. Hence, I conclude that the data

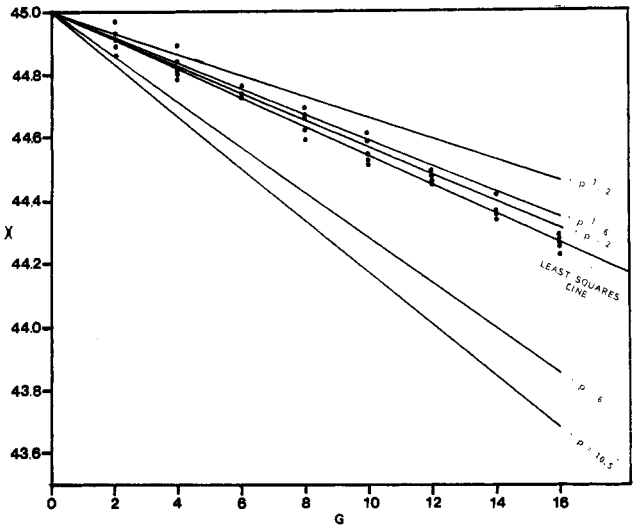

FIGURE 5: Extinction angle χ vs. shear rate G for core particles at 0.6 M ionic strength (encircled point, Figure 2B). The least-squares line corresponds to the rotational diffusion coefficient $D_r = 1.03 \times 10^5\ s^{-1}$. Also shown are theoretical curves based upon experimental $[\eta]$ data for prolate (axial ratio p) and oblate (axial ratio p^{-1}) particles of various degrees of anisometry (see text).

reported here at 0.6 M apply to essentially intact core particles with any dissociation appreciably below this level. This receives further substantiation from the high-salt end of Figure 4 in which a clearly defined falloff in excimer fluorescence intensity occurs only well above 0.6 M, supporting the contention that the core is stable at this salt concentration and changes significantly only with H2A and H2B dissociation around 0.8 M ionic strength. The observation that negligible histone loss occurs at or below ~0.6 M agrees also with the findings of Wilhelm & Wilhelm (1980) and Zayetz et al. (1981).

It is clear from Figure 2 that the optical anisotropies of the high- and low-salt forms of the nucleosome are very different. Since the optical anisotropy comes chiefly from the DNA, this implies a significant difference in DNA conformation or trajectory through the particle under these extreme conditions. For purposes of optical model analysis, I focus on the middle of the three 0.6 M points shown (encircled in Figure 2B).

Zero concentration extinction angle data for the 0.6 M point are given in Figure 5. The data are linear within experimental error over the shear range 0–16 ks^{-1}; the least-squares line in Figure 5 is linear with correlation coefficient $r_{xy} = 0.990$ and a standard regression error in χ of 0.3°. The regression line through the data corresponds to a rotational diffusion coefficient $D_r = 1.03 \times 10^5\ s^{-1}$ by using standard orientation theory [eq 1 of Harrington (1981)]. Since the χ vs. G curve is one of the most sensitive tests for solute polydispersity available from flow birefringence (Harrington, 1967, 1981), I interpret Figure 5 as additional evidence against significant heterogeneity in the nucleosome sample. The flow birefringence data corresponding to the extinction angles of Figure 5 are unexceptional in their shear and concentration dependences and hence are not specifically shown here. They are all essentially linear over the range of variables investigated [see also Harrington (1981)].

Optical modeling analysis of the high-salt point requires calculation of Δn_{int} from the experimental $[n]/[\eta]$ ratio by using eq 1–3 and other theoretical considerations developed earlier (Harrington, 1981). However, eq 1 allows determination of $g_a - g_b$ only as a function of the axial ratio, and additional axial dependence is introduced by eq 3. The overall axial ratio dependence of Δn_{int} is shown in panels A and B of Figure 6 for prolate and oblate ellipsoids, respectively, based

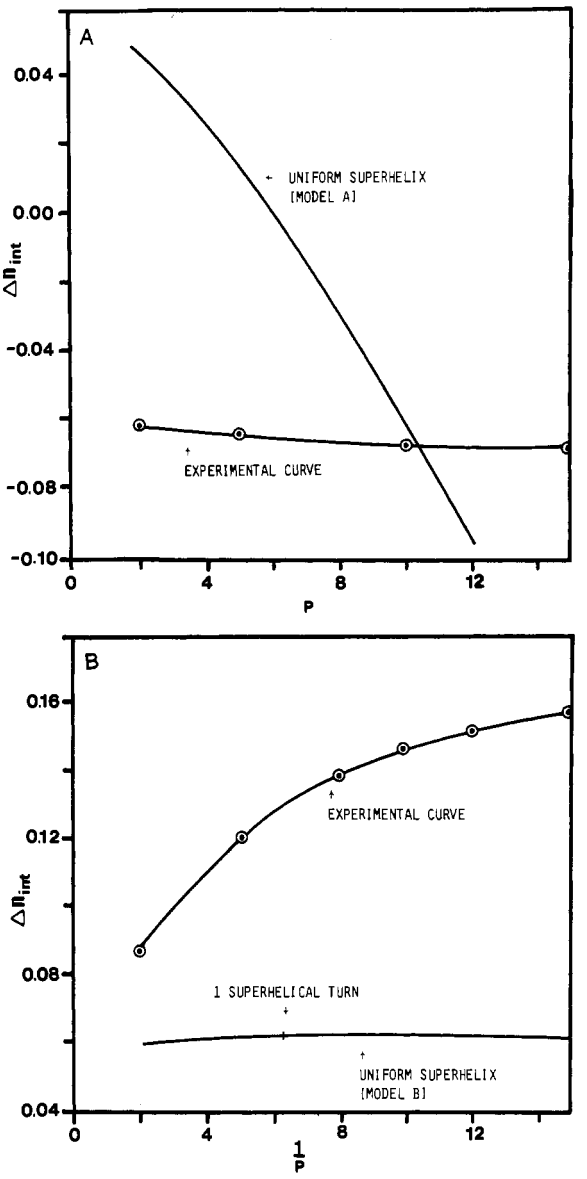

FIGURE 6: Intrinsic birefringence vs. axial ratio for particles of (A) prolate and (B) oblate symmetry. Experimental curves are obtained from $[n]/[\eta]$ and dn/dc data through eq 1–3 (see text). Theoretical curves are for expanded uniform DNA superhelixes, assuming conservation of total volume (models A and B, Figure 7).

upon the experimental value $[n]/[\eta] = -2.181 \times 10^{-8}$ (cgs units) at 0.6 M salt and $dn/dc = 0.184$ (Harrington, 1981). Other experimental parameters were $n = 1.33884$, $\eta_0 = 0.8983 \times 10^{-2}$ P as determined in my laboratory, $M = 2.11 \times 10^5$ (McGhee et al., 1980), and $\bar{v} = 0.661$ as determined at 0.1 M salt with negligible salt dependence around this value (Olins, D. E., et al., 1977; Harrington, 1981).

Optical models considered are presented schematically in Figure 7. Models A and B are uniform DNA superhelixes of prolate and oblate symmetry, respectively, and are identical conceptually with model II of my previous paper (Harrington, 1981) with 146-np DNA of contour length $L = 505$ Å. Helical parameters and intrinsic birefringence are calculated as in the earlier report by using the intrinsic birefringence of DNA, $\Delta n_{int} = -0.1268$, as determined experimentally from flow birefringence (Harrington, 1970b). The axial ratio dependent intrinsic birefringences of the prolate and oblate helixes are shown also in Figure 6A,B. Coincidence between the experimental and model curves occurs for a prolate particle of axial ratio $p = 10.5$ (Figure 6A), but no coincidence occurs for the oblate case

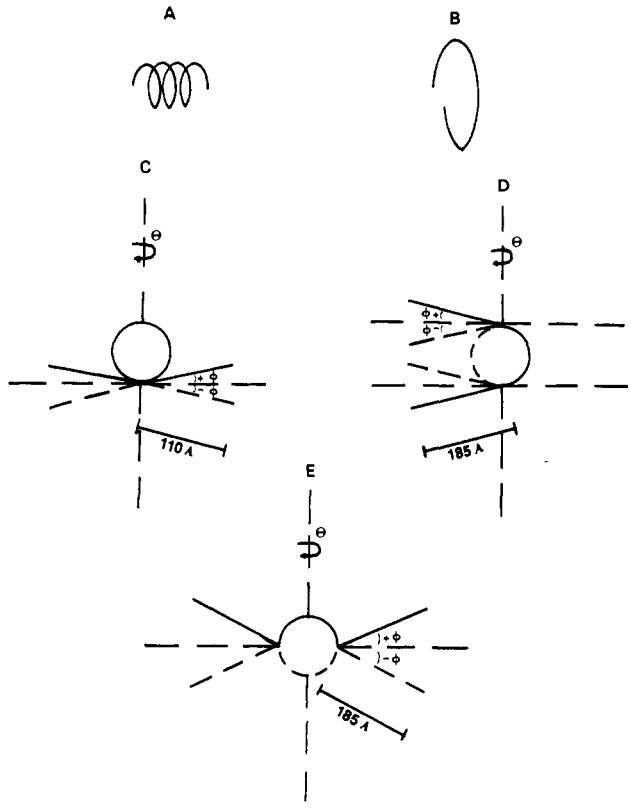

FIGURE 7: Particle conformations used in optical model analyses. Models A and B are respectively uniform prolate and oblate DNA superhelixes, assuming conservation of total particle volume at all ionic strengths. Models C, D, and E are partially unbound states of the physiological ionic strength conformation of the core particle (disk model), assuming loss of DNA–histone binding occurs only along the DNA ends. Model C retains one full superhelical turn of bound DNA about an (assumed intact) histone octamer, leaving ~32 np of unbound regions in either direction. The unbound sections are treated as rigid, B-form DNA of contour length ~110 Å. Models D and E retain one-half superhelical turn of bound DNA, leaving ~50 np of unbound regions of contour length ~185 Å. Model C goes into model D at large negative ϕ values, but the models as shown have different intrinsic birefringences and orient differently in a hydrodynamic velocity gradient. Models C, D, and E may all orient as prolate or oblate particles. The angular variable ϕ is a dihedral angle for the unbound DNA segments, and θ is a torsional or twist angle of the core including bound superhelical DNA (assumed a disk) with respect to the plane of the paper: $\theta = 0°$ when core lies in this plane.

(Figure 6B), at least over the axial ratio range examined (p^{-1} = 2–15). However, agreement is poor between the extinction angle data of Figure 5 and the corresponding theoretical curves for prolate particles of high anisometry.

Alternative representations are shown as models C, D, and E of Figure 7. These are limiting variants of a partially unfolded nucleosomal disk in which the histone core octamer retains its essential integrity, consistent with the results of Figures 1, 3, and 4, and binds only to a central region of the nucleosomal DNA. These models are qualitatively justified by the findings of Van Holde et al. (1980), who report that the central ~100 np of core particle DNA is more strongly bound to the histone core than the ~46 np near the ends. I have treated these models as kinetically rigid structures in solution with the unbound DNA sections rigid and straight. These assumptions seem justified since the histone core will confer structural rigidity to the central DNA region while the unbound ends should approximate free DNA. The experimental chain stiffness of free DNA is quite large (Harrington, 1978). Rizzo & Schellman (1981) have recently determined the absolute high salt persistence length of DNA as 465 Å. From this value, a 110-Å DNA section would, on the average, curve through only 16° of arc and an 185-Å section through 27°. Neither case represents a significant limitation to the models proposed here. Orientations of the unbound DNA and of the intact histone core (with 0.5–1 superhelical turn of bound DNA) are given with respect to the principal axes defined by particle symmetry through the angles ϕ and θ, respectively. In Figure 7, ϕ is a dihedral angle of the free DNA ends with respect to the core; θ is the twist angle of the core with respect to the unbound DNA and ranges from 0° when the disk lies in the plane of the paper to 90° when it is normal to this.

Intrinsic birefringences, Δn_{int}, were calculated for models C, D, and E on an HP-85 computer, assuming applicability of eq 4 and the tensoral additivity of the principal polarization components γ_i. The linear and superhelical regions were considered separately along each principal dimension. Fractional contributions to γ_i from each region were computed as the product of the length fraction and the γ_i for that region, and the total γ_i was obtained as the sum of these fractional contributions. The polarizations of the linear DNA regions were obtained by using eq 4 and the principal refractive index components determined experimentally in an earlier work (Harrington, 1970b). Contributions of the superhelical regions of the DNA to γ_i were computed as described previously (Maestre & Kilkson, 1965; Harrington, 1981), and as in the earlier work, the anisotropy of the histone core was neglected in comparison to that of the DNA. This latter approximation has been discussed (Harrington, 1981), and prior arguments would seem to apply equally well to the present case. All calculations were made in relation to the orientational geometry of the flow birefringence cell in which the light is propagated normal to the plane defined by the velocity gradient and the streamlines of flow. However, it is not clear whether models of the geometries shown orient as quasi-prolate or -oblate particles in a hydrodynamic shear field. Hence, Δn_{int} is obtained as a function of ϕ and θ for both cases.

The actual optical modeling was done as follows. For each model, computer-generated values of Δn_{int} and overall particle dimensions along the three principal geometrical axes were mapped onto a table of θ vs. ϕ at 5° increments in the angular variables. The core twist θ was allowed to range from 0° to 90°. The dihedral angle ϕ was restricted to a range such that each model was geometrically distinct from the others; these limits were −40° to +90° for model C, −50° to +20° for model D, and −80° to +80° for model E. The diameter of free DNA was taken as 20 Å, and the diameter and thickness of the octameric core with bound DNA was taken as 110 and 35 Å, respectively.

The optical models are compared with the experiment in Figure 8A,B. Here, for prolate and oblate symmetries, respectively, regions are mapped inside which Δn_{int} and the overall axial ratio of the models are both within ±10% of the corresponding experimental curves in Figure 6A,B. Regions are identified as to the model and, within each region, the approximate overall axial ratio of the model.

It is clear from Figure 8A that no prolate form of model C can be rationalized experimentally within the stated limits. Since the extinction angle data are most consistent with prolate symmetries of low axial ratio, only the variants of model D with ϕ between −20° and −30° or around +10° and of model E with ϕ near 10° and θ near 90° appear acceptable. None of these possibilities seem satisfactory for the following reasons. At negative values of ϕ, the free DNA segments of model D approach and actually cross at $\phi > -17°$; these are certainly states of high electrostatic repulsion. Positive ϕ values in model

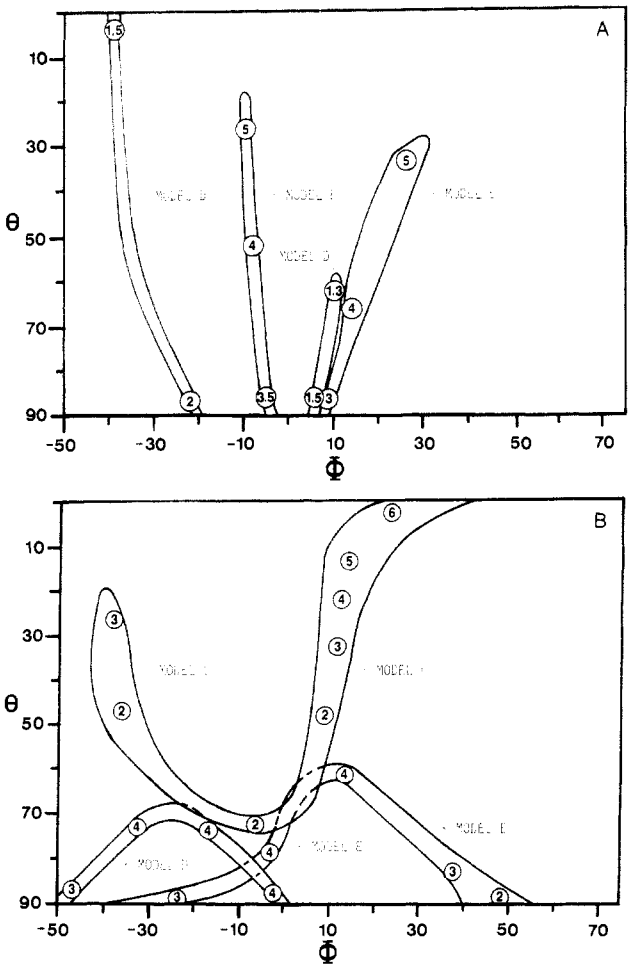

FIGURE 8: Regions in which Δn_{int} and the overall axial ratio for models C, D, and E are within ±10% of the corresponding experimental values given in Figure 6. Models are assumed to orient as (A) prolate and (B) oblate particles in the hydrodynamic shear field of the flow cell. Approximate overall axial ratios of the models in each region of the map, p and p^{-1}, respectively, are shown as encircled numbers. Angular parameters ϕ and θ are as defined in Figure 7.

D are allowed but only for $\theta > 60°$, corresponding to a highly twisted core conformation relative to the straight DNA segments. In addition, the overall anisometry of this model seems too small to rationalize with the observed extinction angles and the relatively large intrinsic viscosity. In like fashion, acceptable conformers of model E all involve θ values near 90°, again corresponding to highly twisted forms.

Similar considerations apply to the oblate conformations of models D and E in Figure 8B. These conformations all involve large values of θ and relatively low oblate anisometries, $p^{-1} < 4$. On the other hand, the lowest θ variants of model C seem physically quite plausible. It is seen from Figure 8B that an acceptable region of model C lies with ϕ in the range −30° to −40° and θ from roughly 20° to 50° and again with ϕ from around 10° to 40° and θ values up to approximately 50°. The latter conformer is particularly interesting since it is essentially that which would be expected from the differential binding studies of Van Holde et al. (1980): tight binding of a central ~100-np DNA to the histone core would lead to an expected conformation in the model C family with $\theta \simeq 0°$ and $\phi \simeq 36°$. In addition, this configuration would be expected to have a relatively high oblate axial ratio as suggested by the theoretical curves in Figure 5.

These optical modeling results may point to conformations of relatively high probability, but the models themselves cannot be taken too literally. Although the assumption of particle rigidity is reasonable on theoretical grounds, the results of Dieterich et al. (1979) imply some degree of flexibility at high ionic strengths. The ±10% acceptability limits in Figure 8 are arbitrary, although these generally represent rather steeply walled valleys with commensurability diminishing rapidly outside these regions. More seriously, however, the axial ratios of the experimental Δn_{int} curves in Figure 6 are based upon rigid ellipsoids of revolution whereas those in Figure 8 are based upon overall dimensions of generally asymmetric models. These quantities are therefore not necessarily functionally equivalent. Moreover, the body of theory used to evaluate Δn_{int} from experimental data is also based upon continuum hydrodynamic and optical theory for rigid, isotropic ellipsoids, and the functional equivalencies between these and the model calculations also are not clear. On the other hand, the experimental data are interpreted by combining related *pairs* of measurements, i.e., $[n]$ with $[\eta]$ in eq 1 and χ with $[\eta]$ in eq 1 and 2 in Harrington (1981) to estimate particle orientation and axial ratio. All these measurements are based upon rotational diffusion, and therefore much of the specific model dependence of the hydrodynamic treatment of the experimental data is thereby removed. Since the optical modeling results presented here seem physically plausible and in substantive accord with other experiments, I believe that the method does indeed yield realistic conformational probabilities of complex anisotropic structures in solution.

Comparison of Hydrodynamic Properties Only for the High-Salt Nucleosome. Sedimentation coefficients for core particles from chicken erythrocytes have been reported over a range of NaCl concentrations by Wilhelm & Wilhelm (1980) and by McGhee et al. (1980). The two sets of results are in agreement at lower salt concentrations but differ at higher salt concentrations, with the latter showing somewhat less falloff in $s_{20,w}$ with increasing NaCl concentrations. Sedimentation of core particles used in this work through 5–25% sucrose gradients at 0.4 and 0.6 M KCl (Figure 3) gave $s_{20,w}$ values in reasonable agreement with the results of Wilhelm & Wilhelm (1980). The observed discrepancies may arise from differences in sample preparations.

The $s_{20,w}$ values of Wilhelm & Wilhelm (1980) are included in Table I and are used with the experimental $[\eta]$ values obtained here to evaluate β in the theory of Mandelkern, Flory, and Scheraga. This parameter has a value of $\beta = 2.12 \times 10^6$ for rigid ellipsoids of low anisometry and increases slowly with increasing axial ratio for prolates but is virtually independent of axial ratio for oblates (Scheraga & Mandelkern, 1953). The corresponding value for chain macromolecules is $\beta = 2.55 \times 10^6$ (Mandelkern & Flory, 1952). It is clear from Table I that β increases numerically with increasing salt concentration over a range 0.4–0.6 M. In terms of simple rigid particle hydrodynamic theory, these results can be rationalized only by assuming an extreme prolate anisometry at high salt concentration, a result which is inconsistent with the analyses of both extinction angles and optical anisotropies given above. Alternatively, β can be fixed at its low-salt value by assuming a salt dependence in $\bar{v}$, but this requires a decrease in $\bar{v}$ with increasing salt concentration, a result which is inconsistent with the known salt dependence of $\bar{v}$ for free DNA (Eisenberg, 1974; McGhee et al., 1980).

The discrepancies in β just noted may arise from differences in samples used for $s_{20,w}$ and $[\eta]$, especially if the $[\eta]$ results reported here were obtained upon partially dissociated core particle samples. All the internal evidence in the present work rules against this. Nevertheless, agreement among laboratories on salt-induced conformational transitions in nucleosomes is

notoriously difficult, and minor variations in sample preparation and handling may be significant. In addition, the partially unfolded nucleosome may be in a metastable state which is difficult to reproduce exactly under slightly different experimental conditions. However, I think it also a reasonable presumption that failure of simple model-dependent hydrodynamic theory in this case is indicative of complex and perhaps asymmetric particle geometry such as that postulated in the optical models used here. Thus, the increases in β with increasing salt concentration shown in Table I may reflect increasing deviation of the actual particle hydrodynamic conformation from the simple rigid ellipsoid of revolution models used in the Mandelkern–Flory–Scheraga theory. If this is the case, it is clear that hydrodynamic properties alone must be interpreted with great care in attempting to understand the architecture of complex systems such as chromatin in solution.

Acknowledgments

I gratefully acknowledge the technical assistance of Kim L. Cairney, who obtained much of the experimental data reported here and assisted with the computer modeling studies. I am also deeply indebted to Dr. Gerald Bunick of the Division of Biology, Oak Ridge National Laboratories, for invaluable advice and assistance in the large-scale production of core particles required for this work and for access to the details of his current preparation methods. I thank also Professor Gerald Fasman for a number of stimulating and helpful discussions leading to useful ideas and Professor Kensal E. Van Holde for a critical reading of the manuscript and for many useful suggestions.

References

Barrett, T. W., & Harrington, R. E. (1977) *Biopolymers 16*, 2167–2188.

Bradbury, E. M., Moss, T., Hayashi, H., Hjelm, R. P., Suau, P., Stephens, R. M., Baldwin, J. P., & Crane-Robinson, C. (1977) *Cold Spring Harbor Symp. Quant. Biol. 42*, 277–286.

Braddock, G. W., Baldwin, J. P., & Bradbury, E. M. (1981) *Biopolymers 20*, 327–343.

Chahal, S. S., Mathews, H. R., & Bradbury, E. M. (1980) *Nature (London) 287*, 76–79.

Crothers, D. M., Dattagupta, N., Hogan, M., Klevan, L., & Lee, K. S. (1978) *Biochemistry 17*, 4525–4550.

Dieterich, A. E., Axel, R., & Cantor, C. R. (1979) *J. Mol. Biol. 129*, 587–602.

Dieterich, A. E., Eshaghpour, H., Crothers, D. M., & Cantor, C. R. (1980) *Nucleic Acids Res. 8*, 2475–2487.

Dixon, G. H., Candido, E. P. M., Honda, B. M., Louie, A. J., Macleod, A. R., & Sung, M. T. (1975) *Ciba Found. Symp. 28*, 229–258.

Eikbush, T. H., & Moudrianakis, E. N. (1978) *Biochemistry 17*, 4955–4964.

Eisenberg, H. (1974) in *Basic Principles in Nucleic Acid Chemistry* (T'so, P. O. P., Ed.) p 171, Academic Press, New York.

Finch, J. T., Lutter, L. C., Rhodes, D., Brown, R. S., Rushton, B., Levitt, M., & Klug, A. (1977) *Nature (London) 269*, 29–36.

Garel, A., & Axel, R. (1976) *Proc. Natl. Acad. Sci. U.S.A. 73*, 3966–3970.

Gill, S. J., & Thompson, D. S. (1967) *Proc. Natl. Acad. Sci. U.S.A. 57*, 562–566.

Gordon, V. C., Knobler, C. M., Olins, D. E., & Schumaker, V. N. (1978) *Proc. Natl. Acad. Sci. U.S.A. 75*, 660–663.

Gordon, V. C., Schumaker, V. N., Olins, D. E., Knobler, C. M., & Horowitz, J. (1979) *Nucleic Acids Res. 6*, 3845–3858.

Harrington, R. E. (1967) *Encycl. Polym. Sci. Technol. 7*, 100–179.

Harrington, R. E. (1970a) *Biopolymers 9*, 159–193.

Harrington, R. E. (1970b) *J. Am. Chem. Soc. 92*, 6957–6964.

Harrington, R. E. (1978) *Biopolymers 17*, 919–936.

Harrington, R. E. (1979) in *Chromatin Structure and Function, Part A* (Nicolini, C., Ed.) pp 167–185, Plenum Press, New York.

Harrington, R. E. (1980) *Biophys. J. 32*, 254–257.

Harrington, R. E. (1981) *Biopolymers 20*, 719–752.

Hewish, D. R., & Burgoyne, L. A. (1973) *Biochem. Biophys. Res. Commun. 52*, 504–510.

Inoue, S. (1961) in *Encyclopedia of Microscopy* (Clark, G. E., Ed.) p 480, Reinhold, New York.

Isenberg, I. (1979) *Annu. Rev. Biochem. 48*, 159–191.

Laemmli, U. K. (1970) *Nature (London) 227*, 680–685.

Libertini, L. J., & Small, E. W. (1980) *Nucleic Acids Res. 8*, 3517–3534.

Lutter, L. C. (1978) *J. Mol. Biol. 124*, 391–420.

Maestre, M. F., & Kilkson, R. (1965) *Biophys. J. 5*, 275–287.

Mandelkern, L., & Flory, P. J. (1952) *J. Chem. Phys. 20*, 212–214.

Martinson, H. G., True, R. J., & Burch, J. E. (1979) *Biochemistry 18*, 1082–1089.

Mathis, D., Oudet, P., & Chambon, P. (1980) *Prog. Nucleic Acid Res. Mol. Biol. 24*, 1–55.

McGhee, J. D., & Felsenfeld, G. (1980) *Annu. Rev. Biochem. 49*, 1115–1156.

McGhee, J. D., Felsenfeld, G., & Eisenberg, H. (1980) *Biophys. J. 32*, 261–269.

Olins, A. L., Breillatt, J. P., Carlson, R. D., Senior, M. B., Wright, E. B., & Olins, D. E. (1977) in *The Molecular Biology of the Mammalian Genetic Apparatus, Part A* (T'so, P. O. P., Ed.) Elsevier/North-Holland, Amsterdam.

Olins, D. E., Bryan, P. N., Harrington, R. E., Hill, W. E., & Olins, A. L. (1977) *Nucleic Acids Res. 4*, 1911–1931.

Oriel, P. J., & Schellman, J. A. (1966) *Biopolymers 4*, 469–494.

Peterlin, A., & Stuart, H. A. (1939) *Z. Phys. 113*, 663–680.

Rizzo, V., & Schellman, J. A. (1981) *Biopolymers 20*, 2143–2163.

Scheraga, H. A., & Mandelkern, L. (1953) *J. Am. Chem. Soc. 75*, 179–184.

Seale, R. L. (1978) *Proc. Natl. Acad. Sci. U.S.A. 75*, 2717–2721.

Siebenlist, V., Simpson, R. B., & Gilbert, W. (1980) *Cell (Cambridge, Mass.) 16*, 269–281.

Stacks, P. C., & Schumaker, V. N. (1979) *Nucleic Acids Res. 7*, 2457–2467.

Van Holde, K. E., Allen, J. R., Tatchell, K., Weischet, W. O., & Lohr, D. (1980) *Biophys. J. 32*, 272–281.

Wasylik, B., & Chambon, P. (1979) *Eur. J. Biochem. 98*, 317–327.

Wasylik, B., Threnin, G., Oudet, P., & Chambon, P. (1979) *J. Mol. Biol. 128*, 411–440.

Weintraub, H., & Grondine, M. (1976) *Science (Washington, D.C.) 193*, 848–856.

Wilhelm, M. L., & Wilhelm, F. X. (1980) *Biochemistry 19*, 4327–4331.
Williamson, P., & Felsenfeld, G. (1978) *Biochemistry 17*, 5695–5705.
Wu, H.-M., Dattagupta, N., Hogan, M., & Crothers, D. M. (1979) *Biochemistry 18*, 3960–3965.
Zama, M., Bryan, P. N., Harrington, R. E., Olins, A. L., & Olins, D. E. (1977) *Cold Spring Harbor Symp. Quant. Biol. 42*, 31–42.
Zayetz, V. W., Bavykin, S. G., Karpov, V. C., & Mirzabekov, A. D. (1981) *Nucleic Acids Res. 9*, 1053–1068.
Ziff, E. B. (1980) *Nature (London) 287*, 491–499.

Conformational Effects of Cation Binding to Myosin and Their Relation to Phosphorylation†

Elissavet Kardami‡ and W. B. Gratzer*

ABSTRACT: Binding profiles of calcium or magnesium ions to rabbit skeletal myosin can be determined from the change in the products of chymotryptic digestion with concentration of the ion. Qualitatively similar effects are brought about by sodium ions at much higher concentrations, and the profiles follow expectations for stoichiometric binding of the univalent ion. The affinity for sodium ions depends on the phosphorylation state of the metal-binding ("regulatory") light chain. The degree of saturation at physiological ionic strength is substantially higher for the phosphorylated form than for the unphosphorylated form. This effect can account quantitatively for the apparent difference in affinity for calcium ions between these two states, measured at physiological sodium ion concentration. Thus if phosphorylation of the light chain leads to a structural perturbation linked to the binding of cations, this may be presumed to come about by way of a net change in occupancy of the cation binding sites rather than through displacement of a resident ion by calcium. A similar pattern of behavior is displayed by cardiac myosin. Like calcium or magnesium, sodium ions are found to protect the proteolytically labile sites in the metal-binding light chain itself and at the head–rod junction, and they promote scission in the putative hinge region, with liberation of heavy meromyosin. The digestion pattern is, under the conditions employed here, unaffected by the state of dispersion of the myosin and is thus not dependent on intramolecular contacts in the filamentous form. If the changes in proteolytic sensitivity in the the head region and at the hinge are indeed reflections of the same binding process, it would follow that the conformational effects of attachment of cations to the light chain are transmitted to the hinge, more than 40 nm away. The existence of separate binding processes in the same range of metal ion concentration cannot, however, be excluded. The stability of skeletal myosin filaments with respect to ionic strength is unaffected by phosphorylation, though only if the metal-binding light chains are undamaged. If they are appreciably degraded, the transition between the monomeric and filamentous states is displaced toward higher ionic strength. The dephosphorylated light chain in situ is much more prone than the phosphorylated to adventitious degradation. With chymotrypsin, only the dephosphorylated light chain gives rise (regardless of whether divalent ions are present or absent) to the intermediate product of scission of M_r 17 000 that still contains the metal ion binding site. When the transition between soluble and filamentous myosins is followed by measurements of turbidity, it is consistently found that dephosphorylated myosin gives rise to a greater turbidity, indicative of the formation of structurally altered filaments.

All known myosins contain low molecular weight subunits, or light chains, certain of which bind divalent metal ions. In invertebrate muscle these subunits are implicated in the capture of calcium ions, released on activation of the muscle, and thus in the regulation of contraction (Szent-Györgyi et al., 1973; Lehman & Szent-Györgyi, 1975; Stafford et al., 1979). The isolated light chain possesses a nonspecific binding site, with comparable affinities for calcium and magnesium, whereas the calcium-specific binding process depends on the association of the regulatory light chain with its heavy chain (Bagshaw & Kendrick-Jones, 1979; Chantler & Szent-Györgyi, 1980). In vertebrate skeletal muscle each myosin contains only a nonspecific metal ion binding site, located on the light chain. At calcium concentrations in the range attained during contraction, these sites would in large measure be occupied by calcium; on the other hand, Bagshaw & Reed (1977) have shown that the rate of displacement of the magnesium ions, with which they were presumed to be associated in the absence of calcium, would be too slow to operate within the time scale of a twitch.

A further property of vertebrate skeletal "regulatory" light chains is that, like those of smooth muscle, they are prone to phosphorylation in vivo, the phosphoryl group being introduced and detached by a specific calcium-activated light chain kinase and a phosphatase, respectively (Pires & Perry, 1977; Morgan et al., 1976). Phosphoryl turnover has been shown to accompany the contraction–relaxation cycle (Bárány et al., 1979). By contrast with its effect in smooth muscle [Chacko et al. (1977), but see also Persechini et al. (1981)], phosphorylation of the striated muscle light chain is not required for actin activation of ATPase. It does not change the myosin ATPase (Morgan et al., 1976), though an enhancement of ATPase activation by regulated actin filaments has been reported (Pemrick, 1980). Phosphorylation causes a small but readily measurable diminution in the affinity of the light chain for calcium, though not for magnesium, in both the isolated state (Alexis & Gratzer, 1978) and in situ (Kardami et al., 1980). The functional consequences of these small effects of phosphorylation have yet to be established.

As matters now stand then, the functional role of calcium binding, of phosphorylation, and indeed of the regulatory light chain in general in vertebrate striated muscle is a matter of

† From the Medical Research Council, Cell Biophysics Unit, King's College, London WC2, United Kingdom. *Received November 10, 1981.*
‡ Present address: Institut Pasteur, 75724-Paris, France.

0006-2960/82/0421-1186$01.25/0